Neuron, Vol. 32, 883–898, December 6, 2001, Copyright ©2001 by Cell Press

Dynamics of Spontaneous Activity in Neocortical Slices

Bu-Qing Mao, Farid Hamzei-Sichani, Dmitriy Aronov, Robert C. Froemke, and Rafael Yuste[1]
Department of Biological Sciences
Columbia University
New York, New York 10027

Summary

The flow of activity in the cortical microcircuitry is poorly understood. We use calcium imaging to reconstruct, with millisecond and single-cell resolution, the spontaneous activity of populations of neurons in unstimulated slices from mouse visual cortex. We find spontaneous activity correlated among networks of layer 5 pyramidal cells. Synchronous ensembles occupy overlapping territories, often share neurons, and are repeatedly activated. Sets of neurons are also sequentially activated numerous times. Network synchronization and sequential correlations are blocked by glutamatergic antagonists, even though spontaneous firing persists in many "autonomously active" neurons. This autonomous activity is periodic and depends on hyperpolarization-activated cationic (H) and persistent sodium (Na_p) currents. We conclude that the isolated neocortical microcircuit generates spontaneous activity, mediated by a combination of intrinsic and circuit mechanisms, and that this activity can be temporally precise.

Introduction

The mammalian neocortex is a tissue of great complexity (Lorente de Nó, 1922). Its connectivity has been investigated for over a hundred years, yet the nature and basic function of the cortical microcircuitry remains unclear (Douglas and Martin, 1998; Somogyi et al., 1998). Traditional models of cortical function have argued for hierarchical, feedforward processing (Hubel and Wiesel, 1977). Recently, neural network models (Hopfield, 1982) have raised the possibility that the neocortex represents a distributed, feedback circuit and have put the emphasis on the endogenous dynamics of cortical activity (Hebb, 1949; Hopfield and Tank, 1986; Lorente de Nó, 1949), rather than on the input pattern. In fact, correlated activity is found in neocortical circuits during sleep or anesthesia or in the absence of sensory stimulation (Creutzfeldt, 1995; Llinás and Ribary, 1993; Steriade et al., 1993; Tsodyks et al., 1999). In addition, neurons in awake behaving animals display persistent activity during memory tasks (Aksay et al., 2001; Fuster, 1995; Goldman-Rakic, 1995). Although neocortical neurons could be activated by other CNS regions, surgically isolated "slabs" of cortex can also produce activity (Burns et al., 1979), and neocortical brain slices can oscillate under certain circumstances (Sanchez-Vives and McCormick, 2000), suggesting that the cortical microcircuitry by itself might generate persistent activity.

To better characterize the intrinsic dynamics of the cortical microcircuitry, we have investigated whether neocortical brain slices can sustain spontaneous activity. In the past, slices have been used to study the responses of neurons to electrical or pharmacological stimulations. At the same time, EPSPs and IPSPs are routinely recorded intracellularly from neurons in slices even under conditions in which the slice is not stimulated. This suggests that some neurons in a "resting" brain slice must be active spontaneously and raises the issues of what is the nature and the mechanism of this spontaneous activity generated intrinsically by the cortical circuitry.

In this study we use calcium imaging of populations of layer 5 neurons from slices of mouse primary visual cortex to reconstruct, with single-cell resolution and millisecond precision, the action potentials (APs) that they produce spontaneously. To do so, we have taken advantage of the strict correspondence between APs and somatic calcium increases (Smetters et al., 1999). We indeed find that a significant percentage of the neurons are spontaneously active and belong mostly to a subclass of pyramidal cells with thick apical dendrites. This activity can persist for at least several seconds. Using Monte Carlo simulations and interval reshuffling, we conclude that this activity displays statistically significant synchronous and delayed correlations. From the occasional occurrence of coactivations by more than two neurons, we characterize the networks of correlated spontaneous activity and identify the neurons that form part of these networks. We find that these networks, formed by pyramidal cells, can overlap and share neurons and can repeat in the recordings resembling "synfire chains" (Abeles, 1991). These correlations are blocked by APV/CNQX, indicating that they are synaptically produced. At the same time, spontaneous "autonomous" activity persists in APV/CNQX, but is blocked by hyperpolarization-activated cationic (H) and persistent, noninactivating Na current (Na_p) current antagonists. Our data indicate that the cortical microcircuit can generate a diverse repertoire of temporally structured dynamics mediated by both intrinsic and synaptic mechanisms.

Results

Imaging Action Potentials in Populations of Neocortical Cells

We performed 281 experiments in 176 coronal brain slices from P12–P23 mice and imaged the region corresponding to primary visual cortex. Slices were loaded with the acetoxymethyl (AM) ester derivative of the calcium indicator fura-2. Using a double-incubation protocol (Yuste, 2000), we labeled a high proportion of the cells in the slices, as assayed by differential interference contrast imaging (Figure 1A). Both pyramidal and nonpyramidal neurons were stained. The percentage of la-

[1] Correspondence: rmy5@columbia.edu

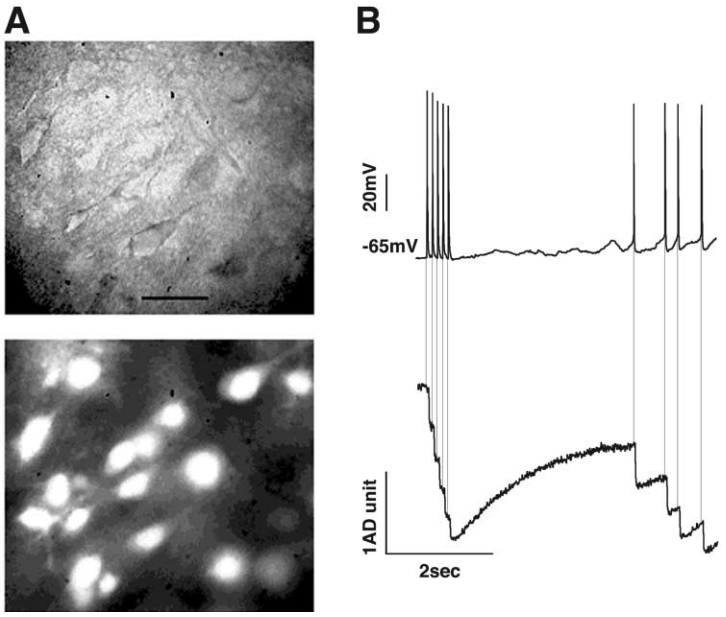

Figure 1. Imaging Action Potentials in Neuronal Populations

(A) Loading of neuronal populations with calcium indicators. Top: DIC image of a visual cortex slice stained with fura-AM. Bottom: fluorescence image of the slice. Note that all cells visible in (A) are loaded with fura. Scale = 50 μm.

(B) Correspondence between somatic calcium transients and APs. Top: whole-cell recordings of a pattern of APs from a neuron. The first five APs were elicited by injecting five pulses of depolarizing current (5 ms, 10 Hz). The last four APs occurred spontaneously. The recording electrode included 100 μM of fura pentapotassium salt. Bottom: Simultaneous imaging of somatic calcium transients from the cell. Lines mark the onset of the calcium transients. Note that each decrease in fluorescence (increase in $[Ca^{2+}]_i$) corresponds to each triggered, as well as spontaneous, action potentials.

beled cells ranged from ~100% to 60%, with smaller percentages at older ages (Peterlin et al., 2000).

To reconstruct the activity of neurons in the slice, we took advantage of the fact that APs produce discrete increases in the somatic concentration of intracellular free calcium ($[Ca^{2+}]_i$) in neurons loaded with fura-2 AM (Smetters et al., 1999). To image spontaneous calcium transients with fast temporal resolution (0.6–2.2 ms) we used an hexagonal photodiode array centered on layer 5. Calcium transients had amplitudes and kinetics similar to those produced in control neurons by APs, triggered by somatic current injections, or occurring spontaneously (Figure 1B, delayed spikes). As shown (Smetters et al., 1999), depolarizations or EPSPs that fell short of causing an action potential failed to produce a detectable calcium transient. These AP-triggered $[Ca^{2+}]_i$ increases are likely due to the opening of somatic voltage-sensitive calcium channels (VSCCs) by sodium spikes because bath application of TTX (2 μM; n = 15 experiments) or the VSCCs antagonists Ni^{2+} (2 mM; n = 10) or Co^{2+} (2 mM; n = 4) blocked all spontaneous calcium transients. We concluded that the spontaneous calcium transients were triggered by APs and mediated by VSCCs and that these calcium transients could be used as reliable indicators that an action potential had occurred in a given cell.

Persistent, Spontaneous Activation of Neocortical Neurons

To characterize the spontaneous activity of the neurons by their calcium transients, we imaged fields of fura-2 AM-labeled neurons (60,154 μm^2; 758 ± 281 cells/mm^2, n = 20). The number of simultaneously imaged cells ranged from 20 to >100. To avoid photobleaching, we restricted imaging to ~18 s "snapshots," during which detection of calcium transients was optimal.

Under standard ACSF at room temperature, many cells showed spontaneous calcium transients (196 experiments; Figure 2). Cells with spontaneous activity ranged from 6 to 31 per imaged field, with an average of 220 ± 67 active cells/mm^2 (n = 20). Thus, approximately 30% of the imaged cells sustained detectable spontaneous activity. Most cells had relatively few calcium transients, with an average interval between transients of 1.1 ± 1.19 s (n = 2160). Similar results were obtained at higher temperatures (~35°C): active cells ranged from 4 to 14 per field, with an average of 166 ± 8 active cells/mm^2 and an average interval between transients of 1.25 ± 2.36 s (n = 1951).

To analyze the spontaneous activity, we reconstructed the pattern of calcium transients by detecting each transient on each photodiode channel and then built rasterplots analogous to those used in multiple electrical recordings (Figures 2B and 2C, and Experimental Procedures). To examine whether the spontaneous activity was episodic, i.e., started and stopped, or whether it was persistent throughout the recordings, we collapsed the rasterplots onto a single line where the activities of all neurons were superimposed (Figure 2C, bottom trace). In almost all experiments the activity was continuous; i.e., seldom were there periods of time in which no activations were detected. The largest gaps found in the collapsed raster plots were ~900 ms, although in most experiments, gaps larger than 50 ms were present. Since we recorded from 20–100 neurons on the surface of the brain slice, whereas approximately 90,000 neurons are present for each mm^3 of mouse cortex (Braitenberg and Schüzt, 1998), it is possible that during the gaps, spontaneous activity persists in the nonimaged region of the slice. We concluded from these data that in standard ACSF, neocortical brain slices are capable of spontaneous activity that can involve a sizable (30%) proportion of neurons in layer 5. This activity can persist in a small cortical territory for at least several seconds, and it may spread through the slice continuously.

Because our data were collected in fura-2 AM-labeled slices, we inquired whether the loading procedure, the

use of fura-2, or the fluorescence excitation were generating artifactual spontaneous activity. We tested this by whole-cell recordings from slices not loaded with fura-2 and not imaged (Figure 3A). Some neurons had spontaneous activity after break-in, as evidenced by their repeated firing of APs. We also found that this activity could disappear within a few minutes of whole-cell recording. To prevent this "washout," we carried out loose cell-attached recordings (LCA) (Barbour and Isope, 2000) from 20 randomly chosen layer 5 pyramidal neurons from 20 different slices and found that 16 cells were silent, whereas 4 showed spontaneous activity, as evidenced by the upwards deflections with short time-to-peak ($<$1 ms), which mimicked the time course of APs (Figures 3B–3E). The percentage of active neurons or the ISIs was not significantly different from those optically detected in fura-2-loaded slices (25% versus 29%; $p > 0.5$; 0.81 $\pm$ 0.78 versus 1.1 $\pm$ 1.19 s; $p > 0.3$, t test). To exclude the possibility that "silent" neurons were merely dead, we made whole-cell recordings on the same cells. Silent cells had normal resting potential <-60mV and, when injected with a 0.5 s pulses of 0.5–0.7 nA, fired robust APs (Figure 3D). These control experiments, performed without fluorescence excitation, indicated that the spontaneous activity was not due to the imaging, the loading procedure, or to the presence of fura-2 in the neurons.

Repeated Activation of the Same Population of Cells

We then characterized the spontaneous activity found in our imaging experiments. To quantify to what degree the imaged spontaneous activity persisted in the same cells, we performed two-trial experiments in which two 9 s optical recordings of the same cells were separated by several (5–22) minutes. Specifically, we examined whether cells that were active in one trial were also active in the other trial by computing forward (F) and backward (B) repeatability (in %) as, $F = N_{12}/N_1$ and $B = N_{12}/N_2$, where N_1 is the number of active cells recorded in trial one, N_2 the number in trial two, and N_{12} the number of cells active in both trials. We did not find significant differences in F and B ($F = 81 \pm 13\%$ and $B = 83 \pm 12\%$, $n = 28$ experiments; average number of active cells = 11.2 $\pm$ 5.4 for N_1 and 10.9 $\pm$ 5.6 for N_2). The level of spontaneous activity also did not change from trial to trial (0.816 $\pm$ 0.52, $n = 255$ versus 0.779 $\pm$ 0.47, $n = 255$ activations/s). Thus, most of the spontaneously active cells remain active for at least several minutes.

Spontaneously Active Cells Are Mostly Large Pyramidal Neurons

The fact that a minority of the imaged cells sustained spontaneous activity and that these cells were repeatedly active in different trials, separated by several minutes, indicated that the spontaneous activity involved a specific class of neurons in layer 5. To identify them, we patched active cells with whole-cell electrodes containing fura-2 pentapotassium salt (100–500 μM), biocytin (0.5%–1%), and, in some experiments, Lucifer yellow ($<$1%). After whole-cell recording was established, we injected current pulses into the cell to elicit APs and their corresponding calcium transients. We confirmed that the patched cell was the same cell that previously showed spontaneous activity by ensuring that the evoked calcium transients occurred in the same photodiode as the one that previously recorded the spontaneous transients (Figures 4A–4C).

These whole-cell recordings confirmed that the imaged cells that displayed spontaneous activity were neurons ($n = 38/38$ Lucifer yellow; 25/25 biocytin). These cells had resting membrane potentials of <-60 mV, APs that overshot zero, and input resistances of 234 $\pm$ 62 MΩ ($n = 13$). The majority of the reconstructed neurons were large layer 5 pyramidal cells ($n = 19$) (Mason and Larkman, 1990), characterized by thick apical dendrites (Figure 4D). These cells can fire bursts of action potentials (Connors and Gutnick, 1990) and may play a special role in cortical synchronization (Connors, 1984). Three neurons, however, displayed nonpyramidal morphologies with symmetric dendritic trees without clear apical dendrites: one was a layer 4 cell (Figure 4E), and one a layer 6 inverted pyramid. Interestingly, layer 5 neurons with thin apical dendrites (Mason and Larkman, 1990) were not encountered, although they are present in mouse V1 (A. Tsiola and R.Y, unpublished data). These data indicate that most spontaneously active neurons belong to a type of pyramidal cells with large apical dendrites.

Spontaneous Activity Can Be Temporally Correlated

The rasterplots of many cells showed correlated activation with simultaneous fluorescence transient onsets (data acquired at 0.6–2.1 ms/frame). To quantify this correlation, we analyzed the rasterplots using statistical tests that characterized the degree of correlation among calcium transients (Figure 5). The paucity of activation events, due to the short recording times and low baseline activation rates (number of calcium transient per cell $<$ 50), made standard cross-correlation analysis impractical, so we created a series of tests specifically designed for low-spike data (see Experimental Procedures) (Schwartz et al., 1998). These tests estimate how likely coactivations might be explained by chance by using Monte Carlo simulations of the data to create a distribution of random coactivations.

In the first analysis (*general correlation test*), we used the number of coactivations in the dataset as test statistic and created random datasets for each cell by temporally shuffling the activation times while keeping constant the number of cells, the number of activations, and the interval between activations within each cell. This generated a distribution of correlated activations in the random datasets that enabled the direct estimation of the p value of the coactivations in real data, i.e., the likelihood that the observed coactivations are due to random activation of the neurons (Figures 5A and 5B). To allow sufficient coactivations to occur in the random datasets, and thus enable the calculation of the test statistic, we defined coactive transients as those occurring within five frames (3–11 ms) of each other, so by synchronous we mean coactive within this time window. Using this test in 13 experiments at room temperature, we found that 11 experiments had $p < 0.05$, and 7 of them had $p < 0.001$. Similar results were ob-

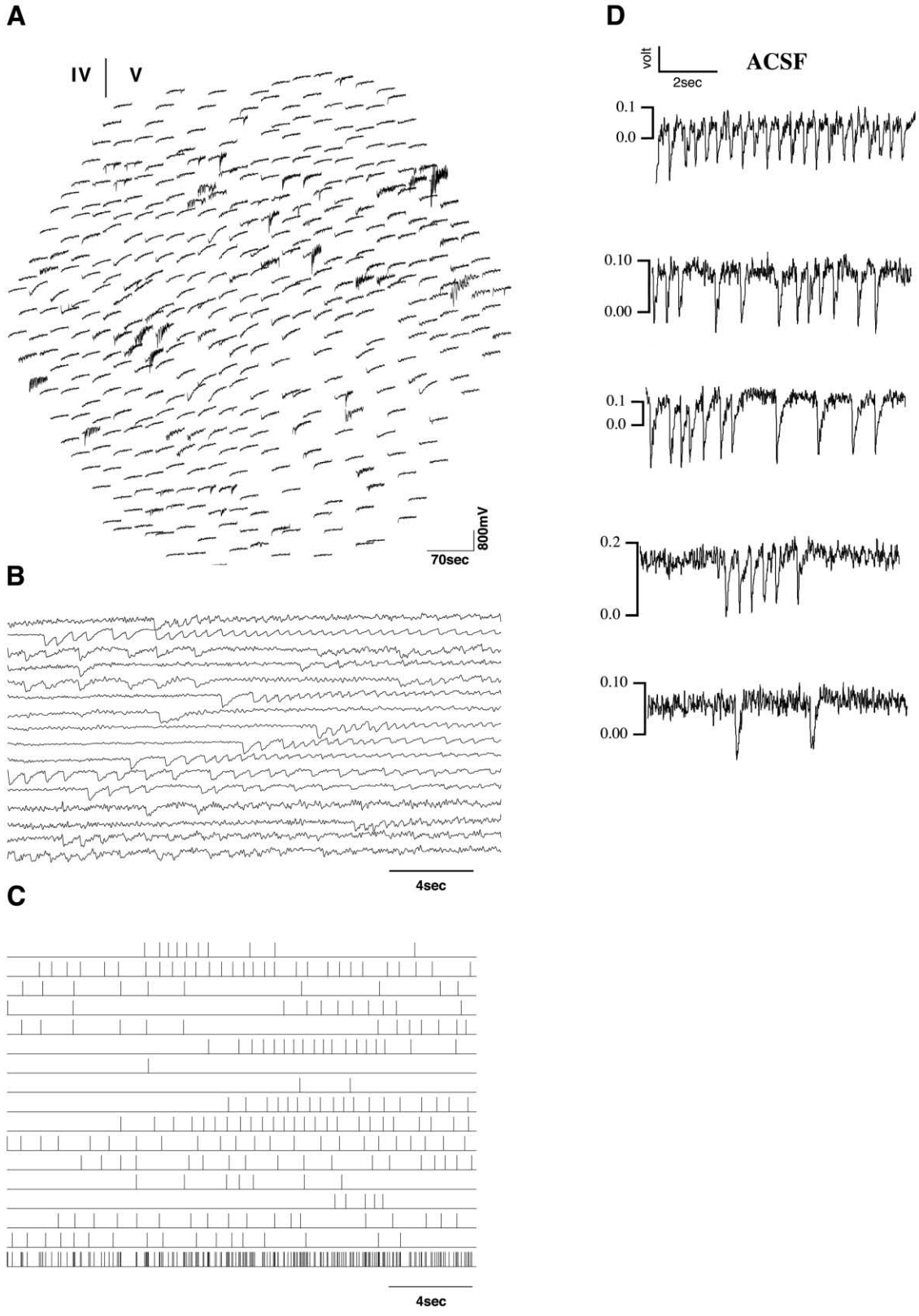

Figure 2. Spontaneous Activity in Unstimulated Brain Slices

(A) Data from the photodiode array. Each trace represents the position and output of a single photodiode, which detects the fluorescence from its corresponding position in the hexagonal field, an area of approximately 11 $\times$ 11 μm. Note that many traces show discrete decreases in fluorescence, indicative of APs.

(B) Selected traces of calcium transients, each from one of the photodiodes shown in (A). Traces have been scaled for ease of viewing.

(C) Rasterplot of analyzed traces shown in (B). Each downward deflection onset in (B) is represented by an individual time marker in (C). The

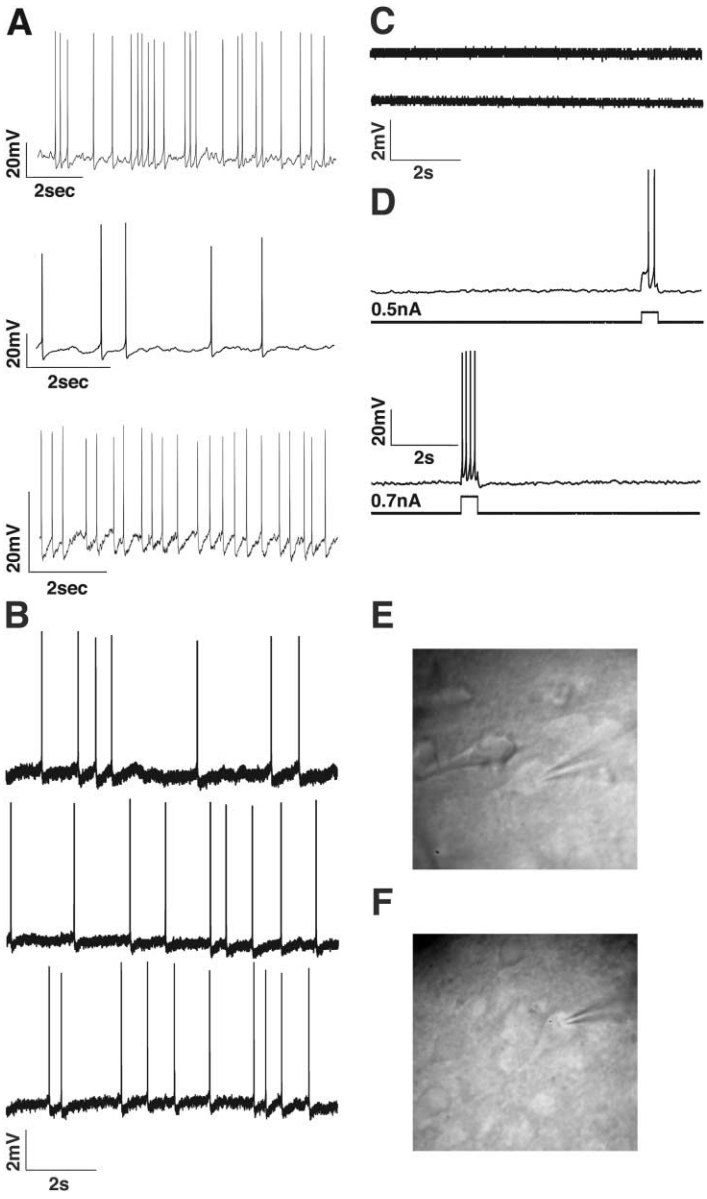

Figure 3. Spontaneous Activity in Unloaded Slices

(A) Whole-cell recordings of spontaneously active cells from unloaded slices. Recordings from three pyramidal cells from unloaded slices. Shortly after break-in, spontaneous AP activity can be detected.

(B) Loose cell-attached recordings from three spontaneously active layer 5 neurons. Notice the upward deflections, extracellular signatures of AP.

(C) Similar recordings from two "silent" neurons do not show upward deflections.

(D) Whole-cell recordings from "silent' neurons. In response to current injection, they fire APs.

(E and F) DIC images of active cells. Note their pyramidal morphologies with prominent apical dendrites.

tained at ~35°C (5/10 experiments with $p < 0.02$). This indicated that the spontaneous activity was indeed correlated because there were many more coactivations than expected by chance.

Networks of Correlated Cells Revealed by Multiple Coactivations

While the previous test indicated that the spontaneous activity was correlated when considered as a whole, it did not highlight which individual cells were correlated. To identify those cells, we used two additional tests that focused on combinations of coactivations that are very unlikely to occur by chance because they involve multiplicative probabilities of occurrence. The first test (*many/once test*) identified incidences in the raster plots where four or more cells were active together. The second test (*two/many test*) detected repeated coactivations between two cells. To estimate to what extent these two types of events could be accounted for by chance, we again used Monte Carlo simulations.

bottom plot combines transients from all the other rasters. Note that the activity persists during the recording.

(D) Representative examples of different temporal patterns of calcium transients in standard ACSF. First, regular pattern: sustained activation with relatively similar intervals between transients. Second, irregular pattern: sustained activation but intertransient intervals vary over time. Third, another example of irregular activation pattern. Fourth, bursting: a short period of activations interspersed with silent periods. Fifth, sparse activation pattern.

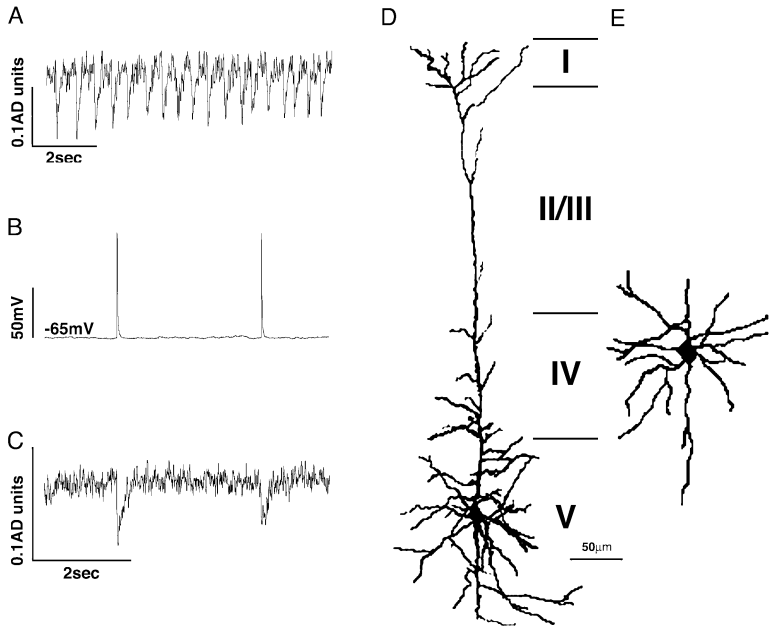

Figure 4. Anatomical Characterization of Spontaneously Active Cells

(A) Spontaneous calcium transients recorded from one of the photodiodes.

(B) The neuron corresponding to the photodiode shown in (A) was patched with an electrode which included 500 μM fura pentapotassium salt. Brief (5 ms) current pulses elicited action potentials.

(C) Corresponding to these action potentials in (B), calcium transients were detected in the same photodiode as in (A).

(D) Biocytin reconstruction of a spontaneously active cell. It is a layer 5 pyramidal cell with a large apical dendrite.

(E) Spontaneously active layer 4 cell.

Using the *many/once* test, we identified coactive groups of four or more neurons in most experiments (10/13 experiments at rt; 5/8 at 35°C; Figures 5C and 5D). These groups were significantly more frequent than in random datasets (7/13 experiments at rt with $p < 0.05$; 6/13 with $p < 0.01$; 3/8 experiments at 35°C with $p < 0.01$). Indeed, in many random datasets, using 1,000 or 10,000 iterations, coactivations of four or more cells were never found, so we reasoned that the coactive groups of four or more cells found in the real datasets likely represented truly correlated networks and used these coactivations to characterize the spatial properties of the networks. On average, each experiment had 5.1 ± 0.6 coactive networks of ≥4 cells (0.021 ± 0.003 networks/cell/s; n = 7, mean ± SEM). These networks had on average 4.3 ± 0.05 cells (36 networks in 7 experiments) which were spatially clustered, with an average distance between cells of 206 ± 14 μm (n = 160) and a mean area of 16,362 ± 987 μm^2 (n = 36). The distribution of these areas was skewed to lower areas with a peak around 5000 μm^2 (data not shown). Interestingly, in experiments in which more than two networks occurred in the same field, we observed that cells, usually pairs or triplets, could be part of more than one network. Specifically, 35 out of 47 networks shared at least one cell with at least one other network, and 25 out of 160 cells took part in at least two distinct networks consisting of subsets of four or more synchronously active cells. Finally, we occasionally observed the exact repetition of the coactivation of all the cells in a network, as if it had precisely reactivated (6/47 networks; Figure 5C, cells 1, 2, 3, and 13).

Further supporting this conclusion, we frequently detected repeated coactivations of two cells (*two/many*; 7/13 at rt; 7/8 at 35°C; Figures 5E and 5F). Multiple coactivations of two cells occurred at significantly higher frequencies than in random datasets (7/13 at rt with $p < 0.01$; 2/8 at 35°C with $p < 0.01$). On average, we detected 13.8 ± 0.8 coactive pairs per experiment, which corresponds to 0.06 ± 0.004 networks/cell/s (mean ± SEM). Similarly to neurons in the coactive networks, cells in a coactive pair were located 217 ± 29 μm from each other (n = 13). These pairs of cells tended to be part of the networks detected in the many/once test, suggesting that they represent different aspects of the same phenomenon (Figure 5F).

Pyramidal Neurons Form Part of the Correlated Networks

We then pursued the anatomical identification of the neurons that were part of the coactive networks. Since most neurons displaying the spontaneous activity were pyramidal neurons with large apical dendrites (Figure 4), we reasoned that the cells in the coactive networks likely belonged to the same group. Nevertheless, it is possible that a subset of cells formed the networks. We investigated this possibility using biocytin to reconstruct cells that were part of a coactive network. We carried out this experiment successfully with four cells from four different slices (Figures 6A and 6B). Three of the neurons were layer 5 pyramidal cells with apical dendrites (Figure 6C), and one was a layer 4 small pyramidal cell. These data confirmed that pyramidal neurons were part of the coactive networks.

Sequences of Delayed Correlations between Cells

Our previous analysis was focused on detecting coactivations, i.e., zero delay correlations. We also wondered if there were nonzero delay correlations in the data that could reveal the flow of activity through the circuit. We pursued this by analyzing the interspike intervals (ISIs; interval between onsets of two calcium transients) between any pair of cells and used the repetitions of the same ISI as an indication of repeated delays of sequential activation of neurons. Indeed, we detected frequent repetitions of the same delays between calcium transients from two neurons (Figures 7A and 7B). To determine whether the number of ISI repetitions with a partic-

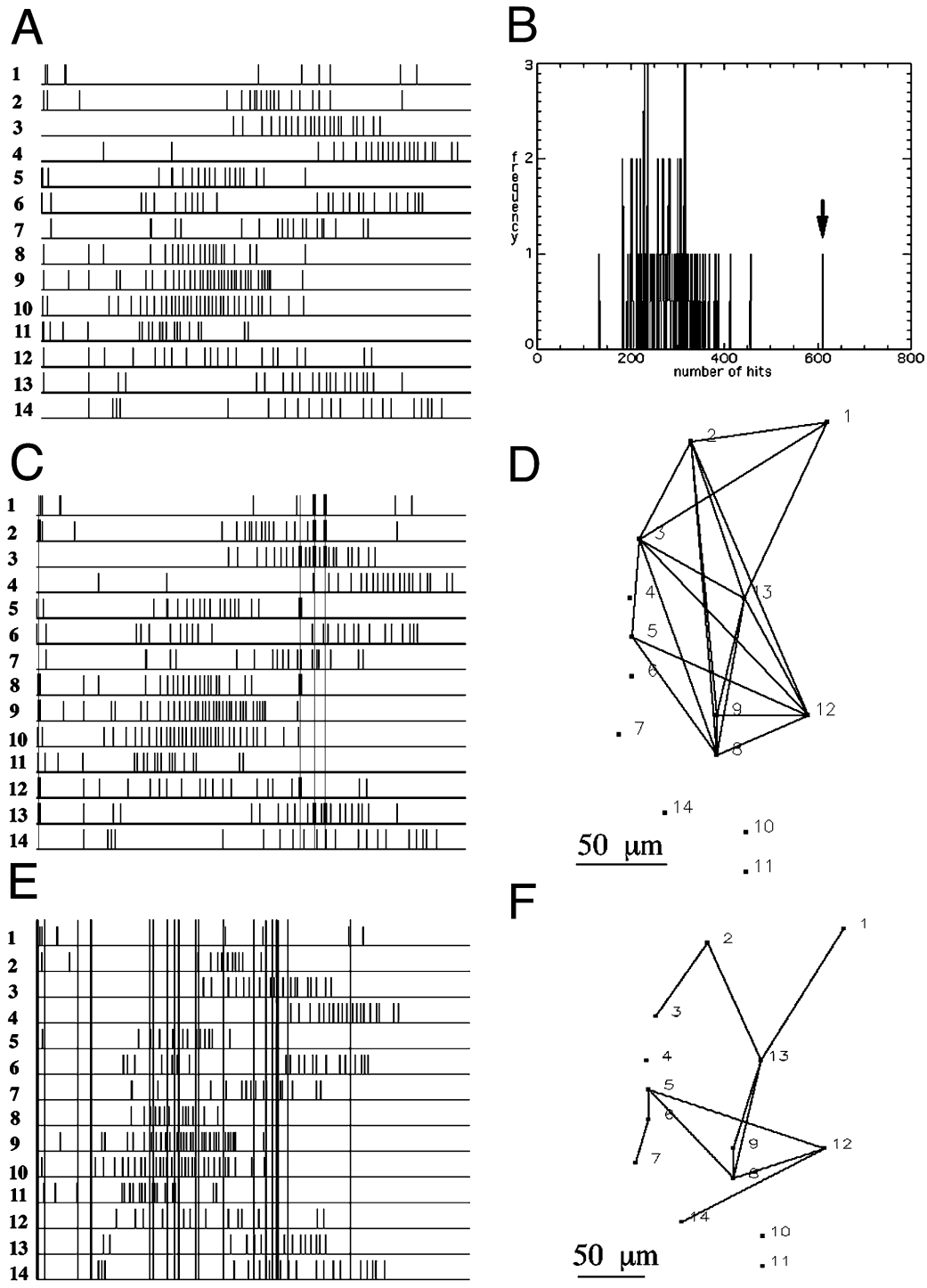

Figure 5. The Spontaneous Activity Is Correlated

(A) Rasterplot of a representative experiment, 18 s in duration. The locations of the neurons in the slice can be seen in panel (D).

(B) Distribution of pairwise correlations found in (A) (arrow) and in a simulated dataset consisting of 1000 Monte Carlo simulations (lines; see Experimental Procedures). Note that the number of coincident events (hits) in the real dataset is greater than those obtained in the simulations.

(C) Many/once analysis: gray vertical lines mark the occurrence of a coactivation of four or more neurons. Thicker tick marks highlight transients that were part of these coactivations. The last two coactivations (cells 1, 2, 3, and 13) repeat exactly.

(D) Correlation map based on the groups of cells activated simultaneously in (C). Lines link those neurons that are part of the coactive networks.

(E) Two/many analysis: vertical lines link pairs of neurons that are coactive more than once.

(F) Correlation map based on the correlated pairs of cells in (E).

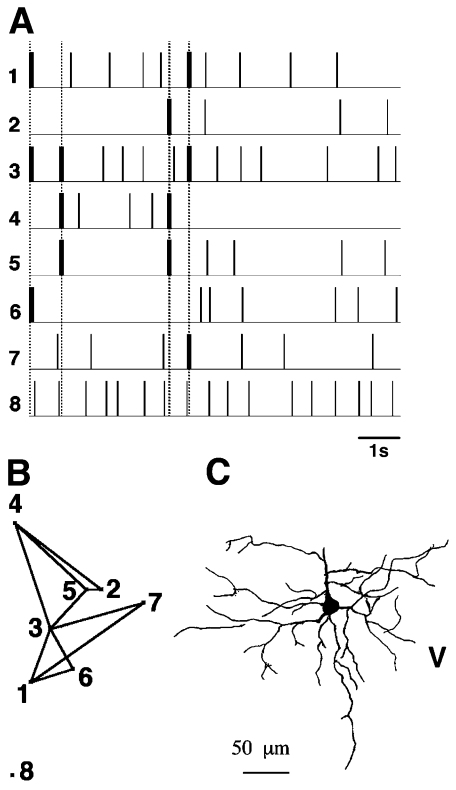

Figure 6. Pyramidal Neurons Are Part of Synchronized Networks

(A) Rasterplots of spontaneous calcium transients from. Dotted lines mark the coincidence activation of at least three cells. Thicker tickmarks highlight transients that were part of these coactivations.

(B) Map of the correlated networks based on (A).

(C) Cell 1 was patched, filled with biocytin, and reconstructed anatomically. The cell is a layer 5 pyramidal neuron.

ular temporal delay was significantly higher than chance, we created pairs of surrogate spike trains by using *interval reshuffling*, a procedure in which ISIs between neighboring spikes in a spike train are randomly reordered (see Experimental Procedures). For each pair of calcium transient trains, we performed interval reshuffling 10,000 times and estimated the p value by comparing the number of exact repetitions found in the real data with that found in the distribution of reshuffled data.

Altogether, we analyzed 193 data sets with 2,400 cells, forming 16,030 pairs. In these pairs, 49 delays were identified by our method as statistically significant with $p < 0.01$ and, of those, 17 were significant with $p < 0.001$. Statistically significant ($p < 0.01$) temporal delays ranged from 0 to 5,122 ms (Figure 7D). The distribution had a peak at zero and declined afterwards (median = 91 ms; mean = 957 ms). The zero peak is due to the fact that a large fraction of the identified connections (15/49, or 30.6%) had a delay smaller than the timing precision window (see Experimental Procedures). Thus, these pairs of cells can be considered as repeatedly coactivated.

Using delays that were statistically significant, we built graphs of the activation pattern of the cells (Figures 7A and 7B). In these graphs we noticed the sequential activation of triplets of cells (Figure 7A, cells 28 before 21 before 22) and the confluent activation of cells (Figure 7B, cells 2 and 9 are coactive before 15). Moreover, in one experiment we detected a firing pattern involving three neurons that repeated nine times, whereby two neurons were coactive and, more than 800 ms later, a third cell was activated (Figure 7C, thick lines). These repeated multineuronal firing patterns, or "precise firing sequences" (Prut et al., 1998), suggest that these detected delayed correlations are not an artifact of the analysis, since sequential or confluent effects are again cases of multiplicative probabilities, unlikely to occur by chance.

Correlations Are Mediated by Glutamatergic Synapses

We next investigated the mechanisms underlying these correlated and sequential coactivations. Since most of the spontaneously active cells were pyramidal neurons, we expected these coactivations to be mediated by excitatory connections. To test this possibility, we imaged the spontaneous activity of slices in the presence of APV/CNQX (50/25 μM) to block NMDA and non-NMDA receptors (Figure 8) and then analyzed these data first for zero delay (correlated) coactivations. The blockade of both types of glutamate receptors with APV/CNQX decreased the zero delay correlations, i.e., increased the p value of the general correlations present in the spontaneous activity (from 0.041 ± 0.09, $n = 13$, to 0.301 ± 0.27, $n = 7$). Indeed, in APV/CNQX, the number of coactive pairs of neurons (two/many) was greatly diminished (from 0.06 ± 0.05 networks/cell/s, $n = 13$, to 0.006 ± 0.009, $n = 7$; t test $p < 0.02$), and only one multiple coactivations (many/once) was detected in seven experiments (from 0.0125 ± 0.016 networks/cell/s, $n = 13$, to 0.001 ± 0.003, $n = 7$). This indicates that the zero delay correlated spontaneous activity was mediated by glutamatergic synapses. Interestingly, APV/CNQX did not significantly affect the number of active cells (12.3 ± 3.4 active cells/trial, $n = 13$, in control ACSF, versus 11.0 ± 1.0, $n = 7$, in APV/CNQX), except that it slightly reduced the average number of calcium transients per cell (0.98 ± 0.32, $n = 13$ versus 0.70 ± 0.34, $n = 7$, not significant t test). We concluded that zero delay-correlated activity was mediated by excitatory synaptic transmission.

To test whether the nonzero delay correlations were also affected by APV/CNQX, we analyzed 37 data sets containing 407 cells that formed 2127 pairs, with the interval reshuffling approach described. Of these pairs, only two delays were correlated with $p < 0.01$ (Figure 7E). Because the fraction of pairs with detected connections was substantially smaller for APV/CNQX data sets, we concluded that nonzero delay correlations, those with repeated temporal delays, were also mediated by synaptic interactions.

Autonomous Activity in APV/CNQX

We were surprised that APV/CNQX did not block all spontaneous activity and focused the rest of the study on understanding the nature and mechanisms of the activity remaining under APV/CNQX, which we termed "autonomous" activity. On visual inspection of the calcium transient rasters from experiments done in APV/

CNQX we noticed that activations became more regular (Figures 8A–8D). To examine whether there were preferred frequencies for activation, we generated histograms of ISIs for data obtained under standard ACSF or APV/CNQX conditions (Figures 8E–8F). Under either condition, the ISI histograms did not contain "bands" that would have indicated preferred ISIs. Nevertheless, the distribution of ISIs was more concentrated under APV/CNQX than under standard ACSF. Indeed, for ACSF the mean ISI was 1.22 ± 1.73 ($n = 2127$) versus 0.69 ± 0.60 ($n = 1521$) for APV/CNQX (t test $p << 0.01$). The median ISI for ACSF was 0.70 versus 0.51 for APV/CNQX (Wilcoxon test $p << 0.01$)

We analyzed the regularity of calcium transients by ISI plots and autocorrelograms to quantify the regularity by the normalized ISI spread (Figure 9; see Experimental Procedures). Transients under standard ACSF and APV/CNQX showed different levels of regularity (for ACSF the mean spread was 1.13 ± 0.66, $n = 172$, versus 0.76 ± 0.35, $n = 149$ for APV/CNQX; $p < 0.001$, t test; and ACSF median 0.92 versus 0.69 for APV/CNQX; $p < 0.001$, Wilcoxon test). ISI spreads before normalization also showed significant difference for ACSF and APV/CNQX (ACSF mean 1.65 ± 1.56 s, $n = 172$, versus 0.78 ± 0.66 s, $n = 149$ for APV/CNQX; $p < 0.001$, t test; and ACSF median 1.11, versus 0.49 for APV/CNQX; $p < 0.001$, Wilcoxon test). We conclude that without glutamatergic transmission, spontaneous activity persists, but with more regular ISIs.

Mechanisms of Autonomous Activity

We then studied the mechanisms underlying the "autonomous" spontaneous activity in the absence of glutamatergic synaptic transmission. In the following experiments, the control condition was ACSF with APV/CNQX. We examined the effect of various pharmacological agents (in addition to APV/CNQX) on the number of transients per second, normalized as the percentage of the activations per second under control condition (Figure 10).

To study whether the inhibitory network influences this form of spontaneous activity, we imaged spontaneous activity in the presence of 25 μM bicuculline methaidodide (BMI), in addition to APV/CNQX. Little change was observed in transient number per second (106% of control; t test, $p = 0.54$). We then proceeded to study intrinsic membrane mechanisms that sustain the persistent activity. In other parts of the nervous system, several currents have been known to underlie repetitive or oscillatory activity: persistent sodium (Na_p), low-threshold calcium current (Crill, 1996; Llinás, 1988), or H-current (Luthi and McCormick, 1996). We first examined the role of low-threshold calcium current by using low nickel concentrations (50 μM). The number of transients under Ni^{2+} decreased to 82% of that under control (t test, $p = 0.46$). More drastic changes were seen with agents that block H current and Na_p current. To block H current, we first used 2–4 mM cesium, but it had no inhibitory effect on the number of transients; indeed the number of transients increased to 110% of control (t test, $p = 0.27$). We reasoned that Cs probably blocked potassium currents. We thus used another H channel blocker, ZD7288 (50–100 μM), which reduced the number of transients to 32% that of control condition (t test, $p < 0.001$). Both pieces of data suggested the involvement of H current in the repetitive activity under APV/CNQX. To study the role of Na_p current, low-dose TTX (15–100 nM) was used and found to block the firing of transients completely (t test, $p < 0.001$). Another blocker of the Na_p current, phenytoin (40 μM), reduced the transient number to 15% of control (t test, $p < 0.001$). These results indicate that H current and Na_p current underlie repetitive activity under APV/CNQX.

Discussion

Single-Cell Resolution Imaging of Neocortical Slices Reveals Spontaneous Activity

We perform the reconstruction of the spontaneous activity pattern in ensembles of cortical neurons in slices with single-cell and millisecond time resolution. This approach, using fast imaging of action potential-triggered calcium transients, developed from our previous studies (Yuste and Katz, 1991; Yuste et al., 1992; Schwartz et al., 1998) is possible because of the bulk loading of slices with acetoxymethyl (AM) esters (Yuste and Katz, 1991; Yuste, 2000) and the strict relation between action potentials and somatic calcium transients of AM-loaded cells (Smetters et al., 1999). This technique has the advantage over other imaging methods, such as voltage-sensitive dyes, in that it affords single-cell resolution. This appears crucial for neocortical studies, given the complexity of the circuitry in which neurons with presumably different functions are intermingled in the same layers.

Using calcium imaging, we detect a rich texture of spontaneous activity in brain slices. Previous studies of neocortical brain slices have relied on electrical stimulation or pharmacological manipulations, such as Mg^{2+}-free ACSF or BMI, which trigger epileptiform events. In addition, oscillations are found in ferret neocortical slices in ACSF with 1 mM Ca^{2+} and 1 mM Mg^{2+} (Sanchez-Vives and McCormick, 2000). In contrast, we report here that unstimulated neocortical slices, in standard ACSF conditions (2 mM Ca^{2+} and 2 mM Mg^{2+}; at rt or 35°C), sustain persistent spontaneous activity. Moreover, this activity can be temporally correlated, revealing groups of synchronized or sequentially activated neurons. This activity is nonoscillatory (Figures 2, 5, and 7) and involves approximately 30% of the imaged cells. Even though we cannot completely rule out that the activity could be influenced by the calcium indicator, we find spontaneous AP activity in layer 5 neurons from unloaded, nonimaged slices (Figure 3).

We conclude that the spontaneous activity is structured because it emerges from a particular class of pyramidal neurons (Figures 4 and 6) and that four independent statistical tests show that correlations are present in the data at frequencies significantly higher than chance activation (Figures 5 and 7). In addition, cells display characteristic nonrandom patterns of activation (Figures 2 and 4), and the same neurons are active in different trials. Moreover, the repetitions of particular sequences of activation (Figures 6 and 7) are very difficult to explain by chance. Finally, an indication that the correlations detected with our tests are not artifactual is that they are blocked by APV/CNQX.

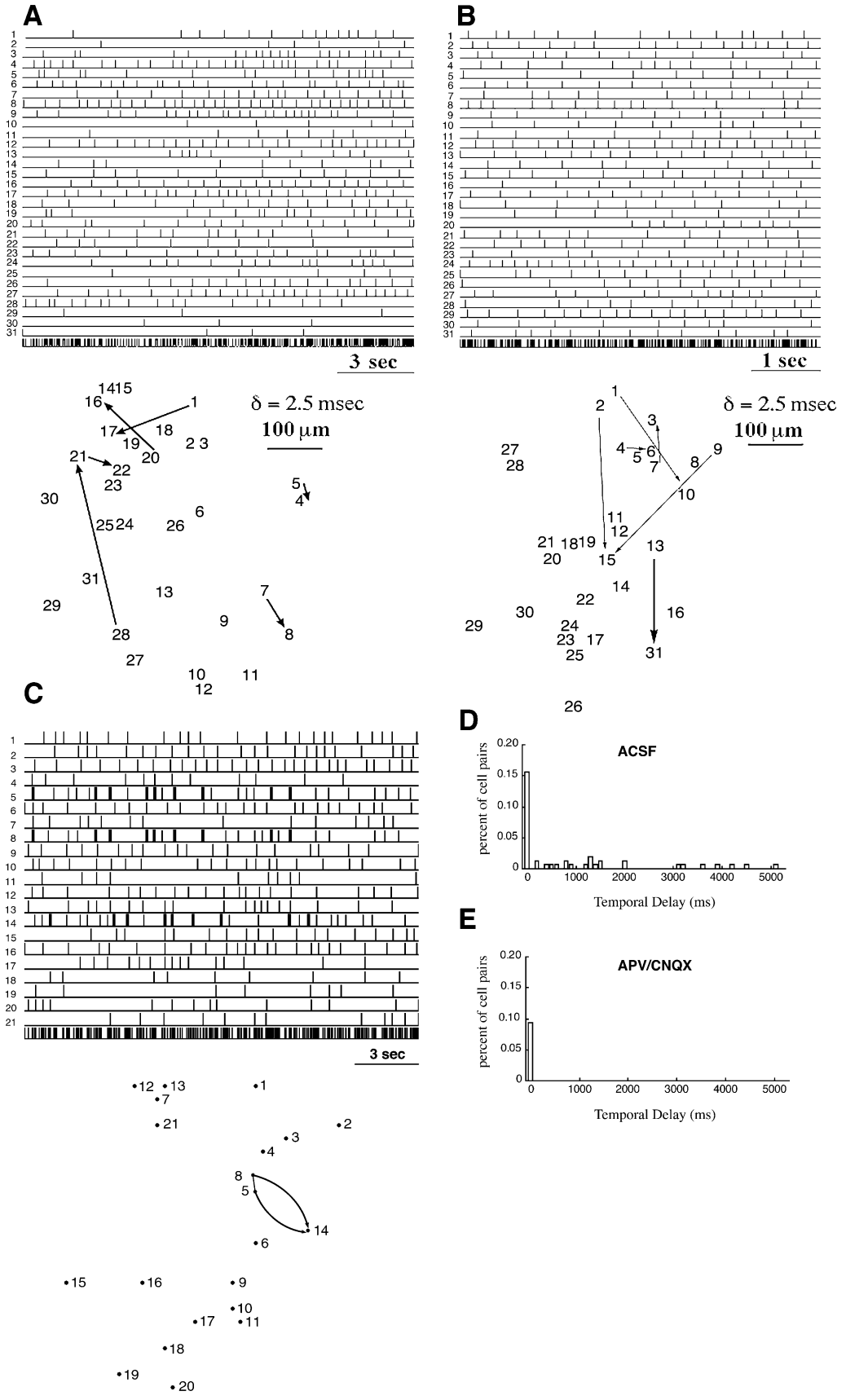
A
3 sec
δ = 2.5 msec
100 μm
B
1 sec
δ = 2.5 msec
100 μm
C
3 sec
D
ACSF
percent of cell pairs
Temporal Delay (ms)
E
APV/CNQX
percent of cell pairs
Temporal Delay (ms)

Temporally Patterned Spontaneous Activity

Our analyses indicate that the spontaneous activity is temporally precise, in the form of both zero and nonzero delay correlations. The correlations that we detect share important similarities with the "synfire chains": hypothesized, synchronized activity that could propagate through the cortical network (Abeles, 1991). These chains would emerge from sequential synchronization of groups of neurons in polysynaptic circuits, and the exact repetition of a precise firing pattern could be the signature of the reactivation of the same circuit. Because of the nonlinearities involved in spike threshold, AP times could be more precise than those of EPSP arrivals ("synchronous gain"), paradoxically eliminating timing jitter with increasing number of synaptic steps (Abeles, 1991). Also, because of the weak effect of any neuron on any other neuron (Markram, 1997), synchronous activity could be favored over nonsynchronous, which might disintegrate in a network of weak connections.

Indeed, we detect synchronization among small groups of neurons, and these synchronized networks can repeat exactly (Figure 5C). We also detect the presence of statistically significant repetitions of precise firing sequences (Prut et al., 1998), even with delays of hundreds of milliseconds and with precision as high as our analysis window (Figure 7C). Although the statistical significance of these correlations is of course subject to the particular model used as the null hypothesis (Oram et al., 1999), we have chosen a strict model in which the ISIs are reshuffled, and we have obtained similar results with Monte Carlo simulations or with spike exchange resampling (Victor and Purpura, 1996). Also, the statistical significance of these events is affected by APV/CNQX, consistent with the possibility that they are circuit based. We feel duty bound to report these results and analyses, even though the mechanisms underlying the correlations, and particularly the long delay correlations, are mysterious and are an important challenge for future research. Moreover, only a clear understanding of these mechanisms will confirm the as yet solely statistical nature of these events.

Regardless of their mechanism and their relation to synfire chains, the coactive and delayed networks that we detect indicate that the cortical microcircuit not only can sustain spontaneous activity, but is capable of generating particular temporal relations between spikes. This precise timing might be related to the processing of information by the cortex. Like musicians in an orchestra, cortical neurons appear to be listening to the firing of other cells to generate precisely timed APs. The fact that we detect these correlations in slices indicates that this hardware seems designed for temporal coding and that internal dynamics could be essential to the computations performed. It may not be a coincidence that the same circuits that are assembled with astonishing precision (Kozloski et al., 2001; Reid and Alonso, 1995) can also generate precise temporal dynamics.

Dual Mechanisms of Spontaneous Activity: Reverberating Circuits and Intrinsic Membrane Properties

In addition to this correlated activity, we find evidence for the existence of an autonomous type of spontaneous activity (Figures 8–10). The neurons responsible for this intrinsically generated activity belong to a subclass of cells that appear identical to the well-studied "thick" layer 5 intrinsically bursting pyramidal neurons in other species (Connors and Gutnick, 1990; Kasper et al., 1994; Mason and Larkman, 1990), although at the ages we studied, they spike regularly (Figure 1). Large layer 5 pyramidal cells are also the origin of major subcortical projections (Kasper et al., 1994), so their activity may exert a particularly strong effect on the rest of the CNS. Their role in the synchronization is prominent (Connors, 1984), perhaps due to their high recurrent collateral projections (Markram, 1997). This high interconnectivity could underlie the principal role of larger layer 5 cells in the spontaneous activity, and the fact that some of these neurons can be spontaneously active under APV/CNQX indicates that they are also intrinsically predisposed to activate spontaneously.

Speculations on the mechanisms that generate spontaneous activity have centered on two ideas: (i) reverberating excitatory circuits (Hebb, 1949; Lorente de Nó, 1949) and (ii) intrinsic, intracellularly generated activity of "pacemaker" cells (Llinás, 1988). These two hypotheses need not be mutually exclusive. Indeed, we find evidence in our data that supports both mechanisms. The blockade of correlated activity seen in APV/CNQX indicates that part of the spontaneous activity is due to excitatory connections, consistent with the idea that these cells are part of reverberating circuits. At the same time, "autonomous" cells still generate action potentials under APV/CNQX via a mechanism that requires Na_p and H-currents. It would be fascinating to explore the role of these neurons and their membrane currents in the behavior of the animal.

Figure 7. Sequential Activation of Neurons

Repetitions of nonzero delay correlated calcium transients in pairs of neurons. Correlated transients between a pair of neurons are detected if the cells are activated sequentially with the same delay several times.

(A) Rasterplot of an experiment (top) and map of the delayed activations in the imaged region (bottom). Arrows link those cell pairs whose delay activation was statistically significant (2.5 ms delay; $p < 0.01$; Monte Carlo; see Experimental Procedures), with the arrow pointing from the first cell to the second. Note how cell 21 is activated after 28, but before 22.

(B) Similar rasterplot and map of a different experiment. Note how cells 9 and 2 are both activated before 15.

(C) Example of delayed correlation involving three cells that repeat nine times. The delayed correlations are significant ($p < 0.01$; interval reshuffling; see Experimental Procedures). Two of the cells (5 and 8) are repeatedly coactivated and both cells are also significantly correlated with cell 14, with temporal delays of 819–828 ms. The analysis window was 22 ms. Transients present in all three cells with the detected delays are shown with thick tickmarks. Note also cases when two out of the three cells are activated with the indicated delays.

(D) Distribution of temporal delays for all significant ($p < 0.01$) correlations found across normal ACSF data sets.

(E) Similar distribution for CNQX/APV data sets.

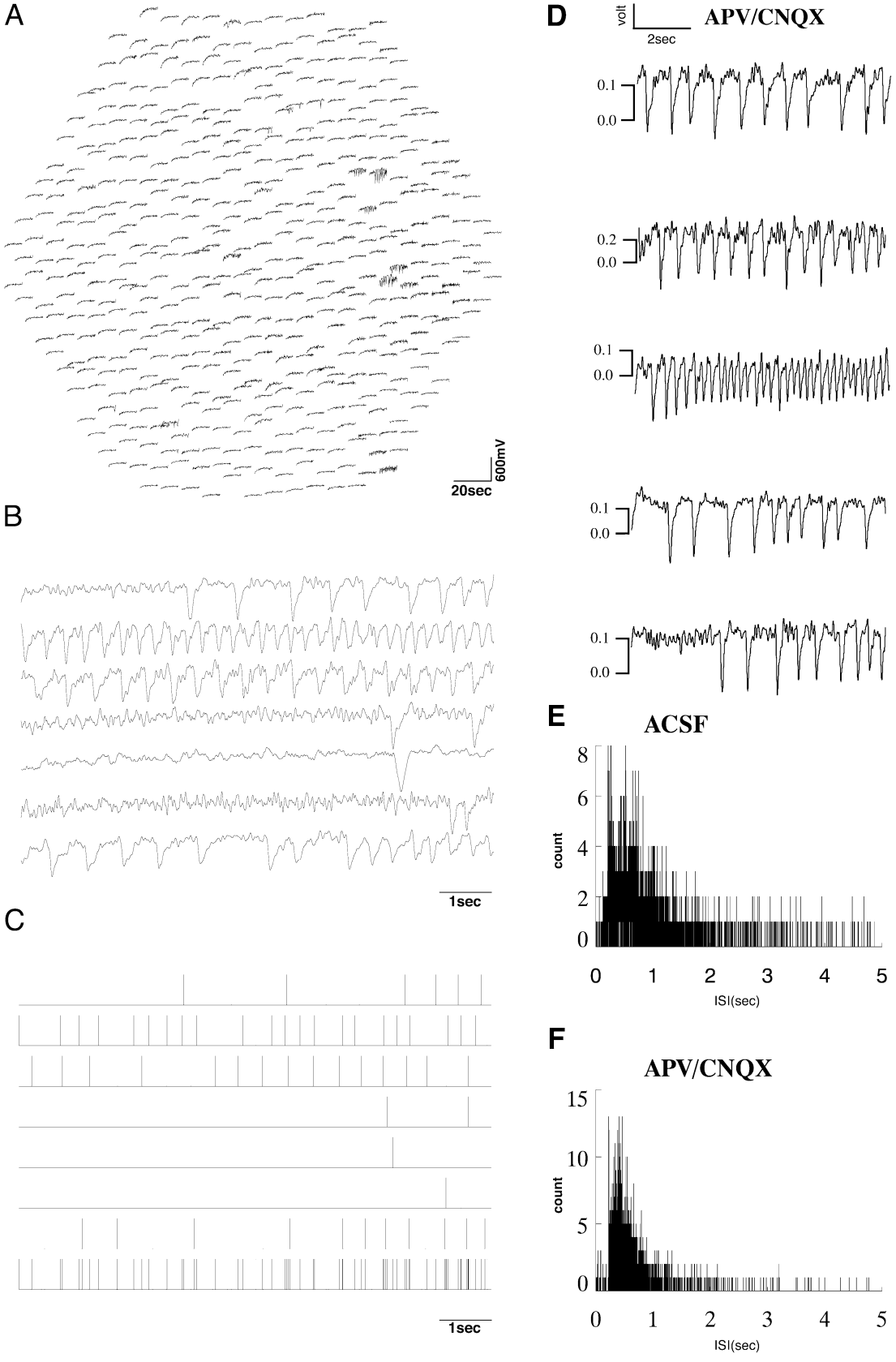
A
600mV
20sec
B
1sec
C
1sec
D
volt
2sec
APV/CNQX
0.1
0.0
0.2
0.0
0.1
0.0
0.1
0.0
0.1
0.0
E
ACSF
count
ISI(sec)
F
APV/CNQX
count
ISI(sec)

Experimental Procedures

Slice Preparation and Imaging

Slices (300 μm thick) were made from primary visual cortices of P12–P23 C57BL/6 mice as described (Peterlin et al., 2000). No differences in results were detected in these ages. The ACSF was (in mM): 126 NaCl, 3 KCl, 26 NaHCO3, 1 NaH2PO4, 2 CaCl2, 2 MgSO4, 10 Dextrose, and bubbled with 95% O^2/5% CO^2. We used a double incubation protocol (Schwartz et al., 1998): (i) an initial incubation with 2–5 μl of a 1 mM fura-2 AM (Molecular Probes; in 100% DMSO) solution for 2 min, and (ii) a second incubation in 3 ml of 10 μM fura-2 AM in ACSF for 60 min. Both incubations were done in the dark. With this protocol we estimate that the neurons were loaded with <50 μM fura-2 (Peterlin et al., 2000).

After loading, slices were placed in a submerged recording chamber on an upright microscope (BX50WI, Olympus). Fluorescent images were taken with a photodiode array (464 detectors, covering 11 μm^2 each; Redshirt Imaging). We used a 380 nm excitation filter, a 395 nm dichroic mirror, a 510 nm emission filter (Chroma), and 40×/0.8 NA or 60×/0.9 NA objectives (Olympus). Signals from the photodiodes were amplified, sampled at 450 to 1600 Hz, and analyzed using Neuroplex (Redshirt Imaging). For short recordings, a pseudo-DC filter with a time constant of tens of seconds was used, whereas for longer recordings, filters were set to time constant of either 180 or 550 ms.

Electrophysiology and Anatomy

Whole-cell patch clamp recordings (BVC-700; Dagan Instruments) were performed using 3–7 MOhm pipettes, filled with (mM): 110–150 K-gluconate of methylsulfonate, 0–20 KCl, 4–10 NaCl, 10 HEPES, 0–5 MgATP, and 0.05–0.5 fura-2 pentapotassium salt (Molecular Probes) with access resistances of 10–20 MΩ. Neurons were filled with patch pipettes containing 0.5%–1% biocytin or 0.1% Lucifer yellow and processed following standard protocols (Peterlin et al., 2000). For demarcation of cortical layers, slices were counterstained before dehydration with Nuclear yellow.

For control experiments (Figure 3), slices were prepared from P12–P14 mice without AM loading. Loose cell-attached (LCA) (Barbour and Isope, 2000) recordings were made by using 3–7 MΩ pipettes, filled with ACSF. Signals were filtered at 1 kHz and digitized at 5 kHz. Experiments were carried out at 32°C. All recordings were done in current-clamp mode. LCA was established by gently touching the pipette against the cell membrane with application of no suction or at times extremely mild negative pressure (<0.1 psi).

Membrane mechanisms underlying spontaneous autonomous activity were examined by using several drugs (SIGMA), including low-dose TTX (15–100 nM), phenytoin (40 μM), cesium chloride (2–4 mM), ZD7288 (50–100 μM; Tocris), nickel chloride (50 μM), and bicuculline methaidodide (BMI, 25 μM).

Statistical Analysis

Measurements are given as mean ± SD, unless noted. Changes in fluorescence were analyzed with programs written in IDL and Matlab. We defined the fluorescence change over time as $\Delta F/F = (F_0 - F_1)/F_0$. We did not encounter consecutive calcium transients of different amplitudes, i.e., optical signals from two different cells, intercalated in the same photodiode recording. For every cell, the onset of each calcium transient was determined using an algorithm that defined the onset as the frame after which the ΔF/F change exceeded a set threshold, typically a negative 5–25 analog-to-digital units (ADU) change per single frame, or a two-step algorithm with consecutive negative changes of 20–30 ADU.

To test whether transients revealed correlations (*general significance test*), we measured the number of simultaneous activations in a recording and used it as a test statistic. We classified events as simultaneous if the onset of their calcium signals occurred within a preset time window (one to five frames). To determine the p value of the statistic, we computed the distribution of the statistic under the null hypothesis of independent transients. To do this, we used Monte Carlo simulations with 100–1,000 replications, which generated a distribution of the test statistic. For each simulation we randomized the beginning of each transient train and wrapped around the end. Thus, the number of cells, number of transients, and exact time intervals between transients were kept constant, and therefore no assumption about the statistical structure of the firing was made. The random numbers used to shift the transient trains were generated using the random generation routines from IDL, based on the Park-Miller algorithm, corrected with a Bays-Durham shuffle. From a histogram of the test statistic, the p value was then calculated as the proportion of the replications in which the test statistic exceeded the test statistic computed from real data. To increase accuracy, we fitted a gaussian function over the replication curve and computed the p value from the fitted curve. These statistical tests compensate for differences in the number of active cells and in the number of calcium transients, because the Monte Carlo simulations are carried out by temporally shuffling the real data.

We performed two additional tests on each dataset: the first test (*many/once test*) detected multiple cells that activated simultaneously and treated the incidence of coactive groups, larger than three cells, over the entire recording as the test statistic. We defined events as simultaneous if the onset of their calcium signals occurred within five frames of each other. The second test (*two/many test*) detected incidences in which groups of cells that were activated simultaneously more than once and used that number as the test statistic, again using a five frame criteria for simultaneity. Monte Carlo simulations, identical to the ones described above, were used in both tests to estimate the significance of those two test statistics.

To identify delayed correlations, for each trace, a Hanning filter with a window size of 101 data points was used and the baseline was then approximated by fitting a cubic function to the maxima of the trace on 10 equal sections of the trace. At each point in time, the average difference of the trace and the baseline was evaluated for 100 consequent data points and the average derivative value was evaluated for 80 consequent data points. Spikes were considered to occur at points in time for which the former value was at least 25% of the minimum and the latter value was at least 20% of the minimum across the entire trace. For each pair of transient trains in a dataset, we identified all ISI repetitions. We then measured the delays between the timings of the transients that participated in these intervals and counted the number of ISI repetitions for each temporal delay. Next, we determined whether the number of ISI repetitions with the identified temporal delay was significantly higher than chance. We created pairs of surrogate transient trains using *interval reshuffling*, a procedure in which ISIs between neighboring transients in a transient train are randomly reordered. The advantage of this method is that it preserves the number of transients and the distribution of intervals, both of which have an effect on the ISI correlation. However, consistent temporal delays between the intervals are not preserved, allowing for an estimation of randomly occurring delayed correlation. For each pair of transient trains, we performed interval reshuffling 10,000 times and counted the number of ISI repetitions with the most commonly occurring delay for each surrogate pair. The p value was directly estimated from the resulting distribution. We performed this analysis for some data sets with various temporal resolutions, ranging from 1 frame (0.6–2.2 ms) to 50 frames (30–110 ms). We chose a temporal resolution of 10 frames (6–22 ms) as a compromise between detection of delayed correlations and estima-

Figure 8. Imaging Spontaneous Activity in APV/CNQX

(A) Spontaneous activity was recorded by photodiode array, displayed as in Figure 2; under ACSF containing APV/CNQX.

(B) Selected traces of calcium transients from (A).

(C) Rasterplots for traces shown in (B).

(D) Examples of different intrinsic patterns of calcium transients imaged in APV/CNQX.

(E) Histogram of ISIs under standard ACSF.

(F) Histogram of ISIs under APV/CNQX. ISIs has a more concentrated distribution under APV/CNQX.

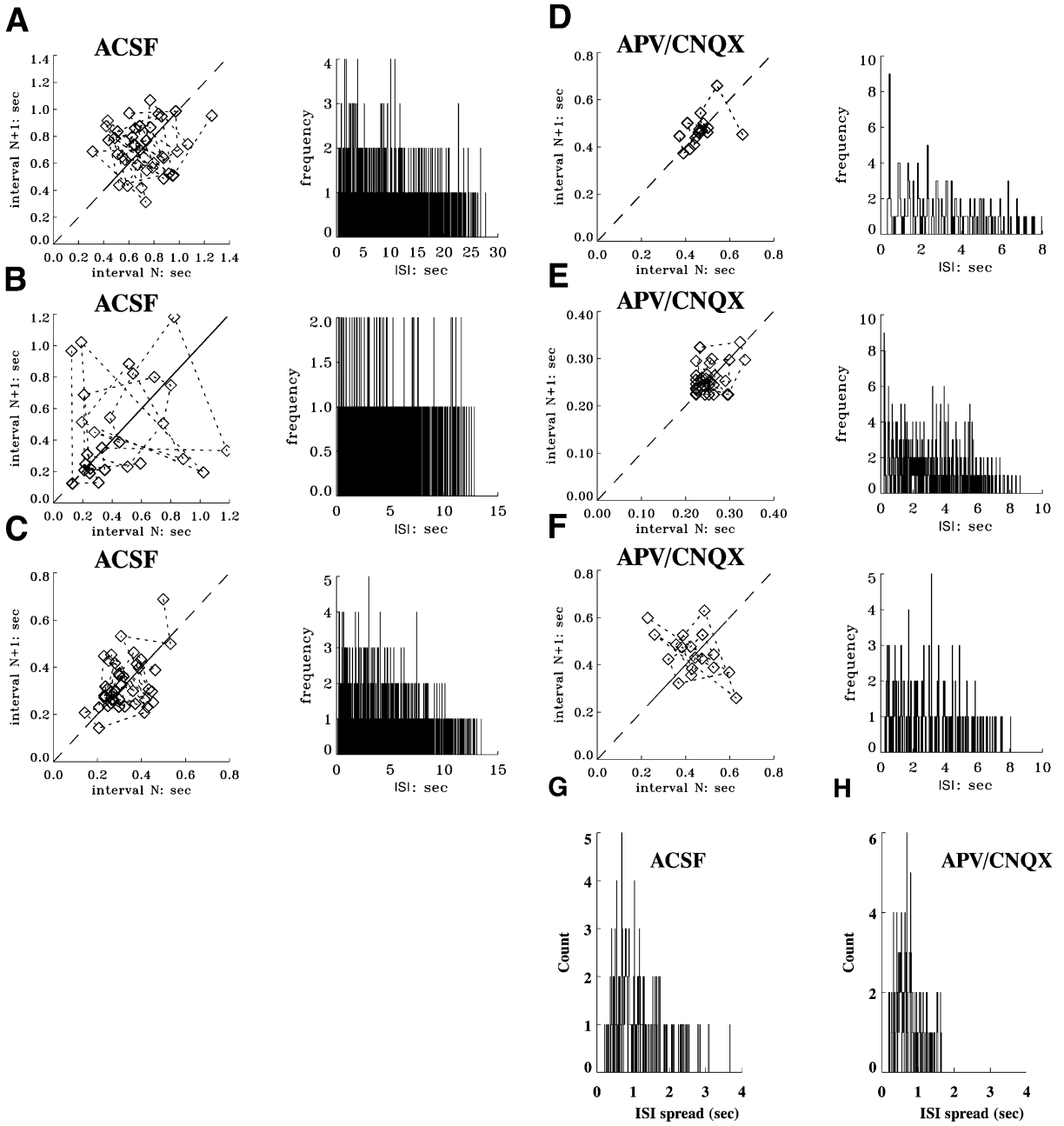

Figure 9. Regularity of ISIs under APV/CNQX

(A–C) ISI plots (left) and autocorrelograms (right) of three transient trains under ACSF.

(D–F) ISI plots and autocorrelograms of three transient trains under APV/CNQX. Transient trains in (D–F) are more regular than those in (A–C).

(G) Histogram of normalized ISI spread (see Experimental Procedures) in ACSF.

(H) Histogram of normalized ISI spread in APV/CNQX.

tion of their significance, which depends on the window chosen (Prut et al., 1998).

We also performed independent analyses of delayed correlations using *spike exchange resample*, which consists of repeatedly exchanging the time position of pairs of spikes randomly chosen from two cells (Victor and Purpura 1996), and *Monte Carlo* simulations, randomizing the time position of each spike (Schwartz et al, 1998). In these two additional tests, we did not find any significant difference in results compared to interval reshuffling (data not shown).

For the analysis of the regularity of calcium transients, we used two types of ISI plots. Suppose that a train has n transients at t = t_1, t_2, t_3, and t_n. The first plot consists of (n − 2) dots with abscissa and ordinate ($t_i - t_{i-1}$, $t_{i+1} - t_i$), i = 2, …n − 1. For a perfectly regular train with period T, the plot collapses to a single point (T, T). For less periodic trains, the ISI plot consists of dots that spread around a center whose coordinates (X_0, Y_0) are determined by minimizing mean square distance from all the dots. The spread of these dots is measured by the square root of the mean square distance and is normalized by dividing the spread by the mean ISI, (X_0 + Y_0)/2. This normalized ISI spread was used to quantify transient train regularity. Samples of such ISI plots are shown in Figures 9A–9F, left plots. A second method to visualize regularity is the autocorrelo-

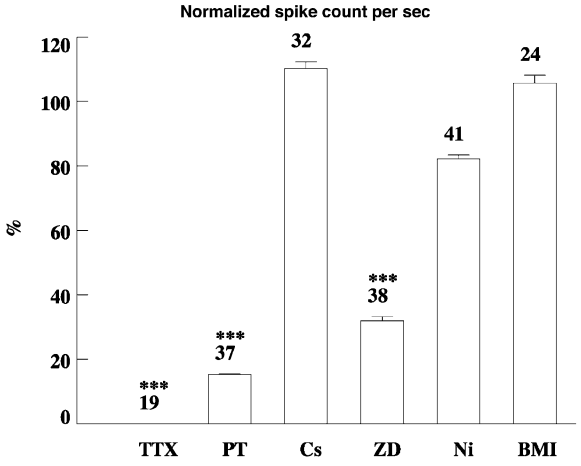

Figure 10. Membrane Mechanisms of Autonomous Activity

Effects of pharmacological antagonists on the spontaneous activity imaged under APV/CNQX ("autonomous"). Control solution also contains APV/CNQX in standard ACSF. TTX (15–50 nM); PT, phenytoin (40 μM); Cs, cesium chloride (2–4 mM); ZD, ZD7288 (50–100 μM); Ni, nickel chloride (50 μM); BMI, bicuculline methaidodide (25 μM). Each bar corresponds to the normalized transient numbers (with the transient number under control solution as 100%). Stars indicate significant differences ($p < 0.001$) in transient numbers under drug versus control conditions. Numbers atop bars are sample sizes.

gram of trains. Specifically, we calculate the difference between the timings of pairs of transients in a train: $ISI_{ij} = t_i - t_j$ (i, j = 1, ...n, $t_i > t_j$). Note, that here ISIs are not limited to between neighboring transients, but between all possible pairs of transients. The regularity of a train can be judged by the shape of the autocorrelogram: if a train is perfectly regular, its autocorrelogram should be triangular in shape, because such a train, with transient number n and period T, will have (n − 1) ISIs of value T, (n − 2) ISIs of value 2T, ..., and one ISIs of value (n − 1)T. If a train is completely random, its autocorrelogram is evenly distributed. Sample autocorrelograms are shown in Figures 9A–9F, right plots.

Acknowledgments

We thank J. Victor for advice and Z. Peterlin and A. Tsiola for help. This work was funded by the NEI and the NINDS.

Received June 11, 2001; revised October 10, 2001.

References

Abeles, M. (1991). Corticonics (Cambridge: Cambridge University Press).

Aksay, E., Gamkrelidze, G., Seung, H.S., Baker, R., and Tank, D.W. (2001). In vivo intracellular recording and perturbation of persistent activity in a neural integrator. Nat. Neurosci. *4*, 184–193.

Barbour, B., and Isope, P. (2000). Combining loose cell-attached stimulation and recording. J. Neurosci. Methods *103*, 199–208.

Braitenberg, V., and Schüzt, A. (1998). Anatomy of the Cortex, Second Edition (Berlin: Springer).

Burns, B., Stean, J., and Webb, A. (1979). The effects of sleep on neurons in isolated cerebral cortex. Proc. R. Soc. Lond. B Biol. Sci. *206*, 281–291.

Connors, B. (1984). Initiation of synchronized neuronal bursting in neocortex. Nature *310*, 685–687.

Connors, B.W., and Gutnick, M.J. (1990). Intrinsic firing patterns of diverse neocortical neurons. Trends Neurosci. *13*, 99–104.

Creutzfeldt, O. (1995). Cortex Cerebri (Oxford: Oxford University Press).

Crill, W. (1996). Persistent sodium current in mammalian central neurons. Annu. Rev. Physiol. *58*, 349–362.

Douglas, R.J., and Martin, K.A.C. (1998). Neocortex. In The Synaptic Organization of the Brain, G.M. Shepherd, ed. (Oxford: Oxford University Press), pp. 459–511.

Fuster, J.M. (1995). Memory in the Cerebral Cortex: An Empirical Approach to Neural Networks in the Human and Nonhuman Primate (Cambridge, MA: MIT Press).

Goldman-Rakic, P.S. (1995). Cellular basis of working memory. Neuron *14*, 477–485.

Hebb, D.O. (1949). The Organization of Behaviour: a Neuropsychological Theory (New York: Wiley).

Hopfield, J.J. (1982). Neural networks and physical systems with emergent collective computational abilities. Proc. Natl. Acad. Sci. USA *79*, 2554–2558.

Hopfield, J.J., and Tank, D.W. (1986). Computing with neural circuits: A model. Science *233*, 625–633.

Hubel, D.H., and Wiesel, T.N. (1977). Functional architecture of the macaque monkey visual cortex. Proc. R. Soc. Lond. B Biol. Sci. *198*, 1–59.

Kasper, E., Larkman, A., Lubke, J., and Blakemore, C. (1994). Pyramidal neurons in layer 5 of the rat visual cortex. I. Correlation among cell morphology, intrinsic electrophysiological properties, and axon targets. J. Comp. Neurol. *339*, 459–474.

Kozloski, J., Hamzei-Sichani, F., and Yuste, R. (2001). Stereotyped position of local synaptic targets in neocortex. Science *293*, 868–872.

Llinás, R.R. (1988). The intrinsic electrophysiological properties of mammalian neurons: insights into central nervous system function. Science *242*, 1654–1664.

Llinás, R., and Ribary, U. (1993). Coherent 40-Hz oscillation characterizes dream state in humans. Proc. Natl. Acad. Sci. USA *90*, 2078–2081.

Lorente de Nó, R. (1922). La corteza cerebral del ratón. Trab. Lab. Invest. Bio. *20*, 41–78.

Lorente de Nó, R. (1949). Cerebral cortex: architecture, intracortical connections, motor projections. In Physiology of the Nervous System, J.F. Fulton, ed. (New York: Oxford University Press), pp. 228–330.

Luthi, A., and McCormick, D. (1996). H-current: properties of a neuronal and network pacemaker. Neuron *21*, 9–12.

Markram, H. (1997). A network of tufted layer 5 pyramidal neurons. Cerebr. Cortex *7*, 523–533.

Markram, H., Lubke, J., Frotscher, M., Roth, A., and Sakmann, B. (1997). Physiology and anatomy of synaptic connections between thick tufted pyramidal neurones in the developing rat neocortex, J. Physiol. (Lond.) *500*, 409–440.

Mason, A., and Larkman, A. (1990). Correlations Between Morphology and Electrophysiology of Pyramidal Neurons in Slices of Rat Visual Cortex. II. Electrophysiology. J. Neurosci. *10*, 1415–1428.

Oram, M.W., Wiener, M.C., Lestienne, R., and Richmond, B.J. (1999). Stochastic nature of precisely timed spike patterns in visual system neuronal responses. J. Neurophysiol. *81*, 3021–3033.

Peterlin, Z.A., Kozloski, J., Mao, B., Tsiola, A., and Yuste, R. (2000). Optical probing of neuronal circuits with calcium indicators. Proc. Natl. Acad. Sci. USA *97*, 3619–3624.

Prut, Y., Vaadia, E., Bergman, H., Haalman, I., Slovin, H., and Abeles, M. (1998). Spatiotemporal structure of cortical activity: properties and behavioral relevance. J. Neurophysiol. *79*, 2857–2874.

Reid, R.C., and Alonso, J.-M. (1995). Specificity of monosynaptic connections from thalamus to visual cortex. Nature *378*, 281–284.

Sanchez-Vives, M., and McCormick, D. (2000). Cellular and network mechanisms of rhythmic recurrent activity in neocortex. Nat. Neurosci. *3*, 1027–1034.

Schwartz, T., Rabinowitz, D., Unni, V.K., Kumar, V.S., Smetters, D.K.,

Tsiola, A., and Yuste, R. (1998). Networks of coactive neurons in developing layer 1. Neuron *20*, 1271–1283.

Smetters, D.K., Majewska, A., and Yuste, R. (1999). Detecting action potentials in neuronal populations with calcium imaging. Methods *18*, 215–221.

Somogyi, P., Tamas, G., Lujan, R., and Buhl, E. (1998). Salient features of synaptic organisation in the cerebral cortex. Brain Res. Brain Res. Rev. *26*, 113–135.

Steriade, M., McCormick, D.A., and Sejnowski, T.J. (1993). Thalamocortical oscillations in the sleeping and aroused brain. Science *262*, 679–685.

Tsodyks, M., Kenet, T., Grinvald, A., and Arieli, A. (1999). Linking spontaneous activity of single cortical neurons and the underlying functional architecture. Science *286*, 1943–1946.

Victor, J.D. and Purpura, K.P. (1996) Nature and precision of temporal coding in visual cortex: a metric- space analysis. J Neurophysiol. *76*, 1310–1326.

Yuste, R. (2000). Loading populations neurons in slices with AM calcium indicators. In Imaging Neurons: A Laboratory Manual, R. Yuste, F. Lanni, and A. Konnerth, eds. (Cold Spring Harbor, NY: Cold Spring Harbor Press), pp. 34.1–34.9.

Yuste, R., and Katz, L.C. (1991). Control of postsynaptic Ca2+ influx in developing neocortex by excitatory and inhibitory neurotransmitters. Neuron *6*, 333–344.

Yuste, R., Peinado, A., and Katz, L.C. (1992). Neuronal domains in developing neocortex. Science *257*, 665–669.